Statistical study of the effect of ULF fluctuations in the IMF on the cross polar cap potential drop for northward IMF

H.-J. Kim,[1] L. Lyons,[1] A. Boudouridis,[2] V. Pilipenko,[3] A. J. Ridley,[4] and J. M. Weygand[5]

Received 11 June 2011; revised 6 August 2011; accepted 12 September 2011; published 15 October 2011.

[1] Recent studies showed that, regardless of the orientation of the Interplanetary Magnetic Field (IMF), ULF wave activity in the solar wind can substantially enhance the convection in the high latitude ionosphere, suggesting that ULF fluctuations may also be an important contributor to the coupling of the solar wind to the magnetosphere-ionosphere system. We conduct a statistical study to understand the effect of ULF power in the IMF on the cross polar cap potential, primarily focusing on northward IMF. We have analyzed the Assimilative Mapping of Ionospheric Electrodynamics (AMIE) calculations of the polar cap potential, a IMF ULF index that is defined as the logarithm of Pc5 ULF power in IMF, and solar wind velocity and dynamic pressure for 249 days in 2003. We find that, separated from the effects of solar wind speed and dynamic pressure, the average cross polar cap potentials show a roughly linear dependence on the ULF index, with a partial correlation coefficient of 0.19. Highly structured convection flow patterns with a number of localized vortices are often observed under fluctuating northward IMF. For such a convection configuration, it is hard to estimate properly the cross polar cap potential drop, as the enhanced flows around the vortices that may be associated with IMF fluctuations do not necessarily yield a large potential drop. Thus, despite the relatively small correlation coefficient, the linear trend we found gives support to the significant role of IMF ULF fluctuations on the coupling of the solar wind to the magnetosphere-ionosphere system.

Citation: Kim, H.-J., L. Lyons, A. Boudouridis, V. Pilipenko, A. J. Ridley, and J. M. Weygand (2011), Statistical study of the effect of ULF fluctuations in the IMF on the cross polar cap potential drop for northward IMF, *J. Geophys. Res.*, *116*, A10311, doi:10.1029/2011JA016931.

1. Introduction

[2] The polar cap is the region of open magnetic field lines that connect the Interplanetary Magnetic Field (IMF) and the geomagnetic field. As the solar wind flows past the Earth's magnetosphere, a dawn-to-dusk electric field generally forms along the magnetopause and maps to the polar cap creating the cross polar cap potential and driving anti-sunward convection within the polar cap. When the IMF becomes more southward, the interconnection of the solar wind and geomagnetic field is enhanced, increasing ionospheric convection and the electric potential across the polar cap [e.g., *Reiff et al.*, 1981; *Cowley*, 1984]. Thus the cross polar cap potential drop can be approximately a direct measure of the instantaneous coupling strength between the solar wind and the magnetosphere. It is well known that the cross polar cap potential drop is positively correlated with solar wind parameters, such as southward IMF, solar wind speed, and dynamic pressure [e.g., *Reiff et al.*, 1981; *Cowley*, 1984; *Reiff and Luhmann*, 1986; *Boyle et al.*, 1997; *Boudouridis et al.*, 2005].

[3] Recently, ULF wave power in the solar wind was proposed to be an additional factor in controlling the coupling of the solar wind-magnetosphere-ionosphere system. *Kim et al.* [2009] and *Lyons et al.* [2009] showed that enhanced ULF wave power can substantially enhance the convection strength in both the dayside and nightside high latitude ionosphere. This ULF power effect was found to be independent of an observed direct effect from the solar wind speed. *Lyons et al.* [2009] showed some examples of an increase of plasma sheet pressure and substorm occurrence rate during periods of strong ULF wave activity under northward IMF, indicating that ULF wave activity may play an important role in geomagnetic activity.

[4] In this paper, as an extension of *Kim et al.* [2009] and *Lyons et al.* [2009], we present results of a statistical study to examine if enhanced ULF wave activity in the IMF can also contribute to an increase of the cross polar cap potential drop ($\Delta\Phi_{pc}$). We primarily seek the statistical relationship between $\Delta\Phi_{pc}$ and an interplanetary ULF index for northward IMF

[1]Department of Atmospheric and Oceanic Sciences, University of California, Los Angeles, California, USA.
[2]Space Science Institute, Boulder, Colorado, USA.
[3]Space Research Institute, Moscow, Russia.
[4]Center for Space Environment Modeling, University of Michigan, Ann Arbor, Michigan, USA.
[5]IGPP, University of California, Los Angeles, California, USA.

0148-0227/11/2011JA016931

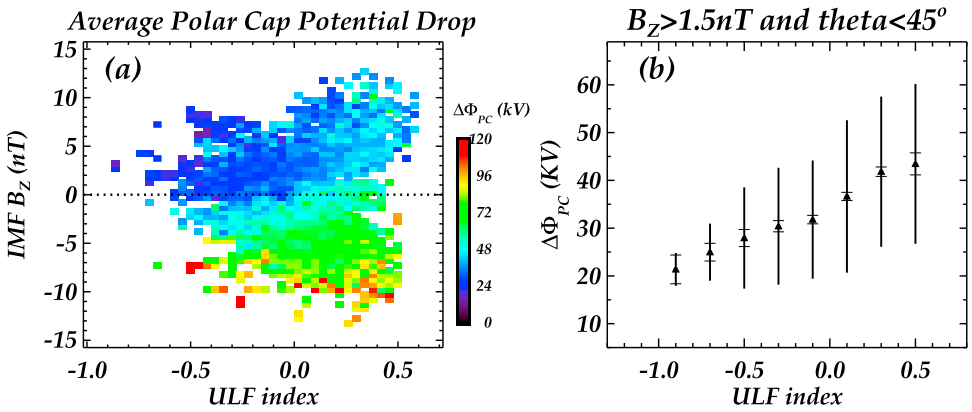

Figure 1. (a) Color-coded average cross polar cap potential versus ULF index and IMF B_z. (b) Bin-averages of all the data points for northward IMF, i.e., the data points with IMF $B_z > 1.5$ nT in Figure 1a. The triangles represent the bin-averages with bin width of 0.2 ULF index, and the bars indicate the standard deviation of the data points in each bin. The 95% confidence interval for each bin-average is indicated by the horizontal ticks on the bars.

with IMF B_z > IMF $|B_y|$, and after suppressing the effects of solar wind speed and solar wind dynamic pressure.

2. Data Description

[5] Cross polar cap potentials derived by the Assimilative Mapping of Ionospheric Electrodynamics (AMIE) technique are used [*Ridley and Kihn*, 2004]. The AMIE technique [*Richmond and Kamide*, 1988] can utilize a large number of observations from various sources (ground magnetometers, DMSP satellites, and radars) to determine the transpolar potential. However, the data from satellites and radars are not always available; therefore in our statistical study for consistency we examine AMIE runs of 1-min resolution that used only ground magnetometers (with 120–140 contributing stations throughout 2003). The cross polar cap potentials are available at http://herot.engin.umich.edu/~amie/data/indices/.

[6] To represent the level of ULF wave activity in the IMF, we use the interplanetary ULF index which has been recently introduced by *Kozyreva et al.* [2007]. The hourly IMF ULF index is defined as the logarithm of the average ULF power in the frequency range of 2 mHz to 7 mHz, and is estimated using time-shifted 1-min IMF data from interplanetary satellites such as Wind and ACE.

[7] For solar wind parameters, we use the ACE and Wind data as time-shifted to the standard position of 17 R_E in front of the magnetosphere by the Weimer technique [*Weimer et al.*, 2003; *Weimer*, 2004]. A 10-min time lag is adopted to account for the travel time of solar wind information from the magnetopause to the ionosphere [*Ridley et al.*, 1998]. For the statistical study, we examine the data described above for a total of 249 days in 2003. The selection criteria for the 249 days are as follows: 1) no large gaps in any data, 2) no significant discrepancy between ACE and Wind solar wind data, 3) no extreme IMF B_z values, i.e., the maximum magnitude of IMF B_z is not greater than 15 nT. By imposing this latter condition, we can exclude the extreme intervals where saturation of cross polar cap potential can be an issue [e.g., *Kivelson and Ridley*, 2008, and references therein]. The prepared data set is of fairly even distribution in seasons, and about the same percentage of the data is associated with either high solar wind speed ($V_{sw} > 550$ km/s for ~52% of the time) or lower solar wind speed streams ($V_{sw} < 550$ km/s for ~48% of the time), which can facilitate unbiased statistics as Pc5 ULF waves are known to be ubiquitous during high speed streams.

[8] As high temporal variations are not of interest here, we obtain 22-min running averages of cross polar cap potentials, and solar wind and IMF parameters from ACE. The hourly ULF index is then interpolated to get values at the same time grids.

3. Statistical Results

[9] Figure 1a shows the color-coded average cross polar cap potential versus IMF B_z and ULF index. For Figure 1a, we first collect the data points (all 22-min running averages) that satisfy one of the three IMF conditions: (A) IMF $B_z > 1.5$ nT and IMF clock angle < 45°, and all the 1-min IMF B_z values within a given averaging window are positive, (B) $|\text{IMF } B_z| < 1.5$nT and $|\text{IMF } B_y| < 0.5$nT, (C) IMF $B_z < -1.5$ nT and IMF clock angle > 135° and all the 1-min IMF B_z values within a given averaging window are negative. Here IMF clock angle, Θ, is defined as $\tan^{-1}(|B_y|/B_z)$ for $B_z > 0$, and $180° - \tan^{-1}(|B_y/B_z|)$ for $B_z < 0$. Conditions (A) and (C) represent predominantly northward or southward IMF with z-component larger than y-component, and Condition (B) represents the IMF B_z fluctuating around 0 with a small amplitude while the average IMF B_y is almost negligible.

[10] In order to capture the average statistical behavior, the cross polar cap potential data are then averaged over grid cells of 0.04 by 0.5 nT in Figure 1a. The color-coded average $\Delta\Phi_{pc}$ clearly shows the well-known increase with the magnitude of southward IMF. However, it is also discernable that for a given IMF B_z (either northward or southward) $\Delta\Phi_{pc}$ gradually increases with increasing ULF wave power, leading to the presence of the same or even slightly larger average $\Delta\Phi_{pc}$ for northward IMF when ULF power is higher than for weakly southward IMF when ULF power is low. Note that the distribution of the data points in Figure 1a is symmetric around $B_z = 0$, indicating the independence of the ULF wave activity level on the IMF orientation.

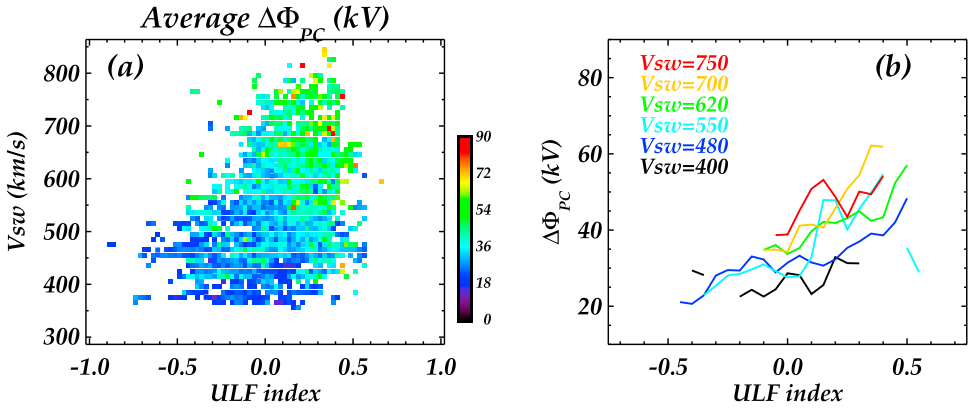

Figure 2. For the data set of northward IMF satisfying Condition (A): (a) color-coded average $\Delta\Phi_{pc}$ versus ULF index and V_{sw}; (b) average dependence of $\Delta\Phi_{pc}$ on ULF index when solar wind speed is fixed at 400, 480, 550, 620, 700, 750 km/s represented by different colors.

[11] To avoid complications in dealing with the southward IMF effect, we primarily focus on northward IMF to find the average relationship between $\Delta\Phi_{pc}$ and ULF index. Figure 1b shows the bin-averages of all the data points satisfying IMF Condition (A), i.e., the data points with IMF $B_z > 1.5$ nT in Figure 1a. In Figure 1b, the triangles represent the bin-averages with bin width of 0.2 ULF index, and the bars indicate the standard deviation of the data points in each bin. The horizontal ticks on the bars indicate 95% confidence intervals for the bin-averages. The bin averages are well aligned on a single line, indicating a roughly linear relation between $\Delta\Phi_{pc}$ and the ULF index.

[12] However, in order to understand the pure relationship between the ULF index and $\Delta\Phi_{pc}$ in Figure 1b, we need to remove the effects of solar wind speed and solar wind dynamic pressure. Not only is the cross polar cap potential positively correlated with these two solar wind parameters, but also the ULF wave activity level is related to solar wind speed, as high speed solar wind streams are usually accompanied by enhanced ULF fluctuations. While the solar wind pressure effect is transient, the solar wind speed effect is more persistent and thus can be important for a long-term statistical study.

[13] To first separate the solar wind speed effect, Figure 2a exhibits color-coded average $\Delta\Phi_{pc}$ versus ULF index and solar wind speed for the northward IMF condition (A). Similar to Figure 1a, all the data points that fall into the same grid cell, now with grid cell size of 0.025 by 10 (km/s), are averaged. The plot shows not only that $\Delta\Phi_{pc}$ increases with V_{sw}, but also that, for a fixed V_{sw}, larger $\Delta\Phi_{pc}$ values could be found in the region of larger ULF index at all solar wind speeds. Note the relation between V_{sw} and ULF power can also be seen, i.e., high solar wind speeds are associated on average with high ULF power. However, enhanced ULF wave power can be observed for both high and low solar wind speeds.

[14] Figure 2b exhibits the average relation between the ULF index and $\Delta\Phi_{pc}$ when solar wind speed is fixed at 400, 480, 550, 620, 700, 750 km/s, which is like cutting through Figure 2a parallel to the x axis. In order to obtain a smoother relation, we take an average of the data points within +/−10 km/s around the six solar wind speeds for each given ULF index grid cell and only plot averages for grid cells having more than 3 data points. Although the lines are not monotonic, we can identify a linear trend for all six solar wind speeds,

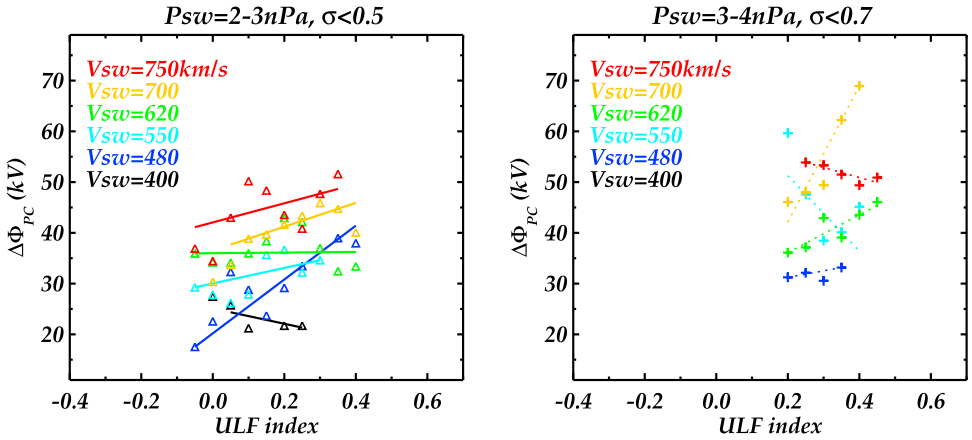

Figure 3. Scatterplot of ULF index versus $\Delta\Phi_{pc}$ for P_{sw} condition of (left) P_{sw} = 2–3 nPa with σ (standard deviation) < 0.5 and (right) P_{sw} = 3–4 nPa with $\sigma < 0.7$, with the symbols "Δ" and "+," respectively. The colors denote the different corresponding V_{sw}, and solid and dashed lines give linear fits for lower and higher P_{sw} conditions, respectively.

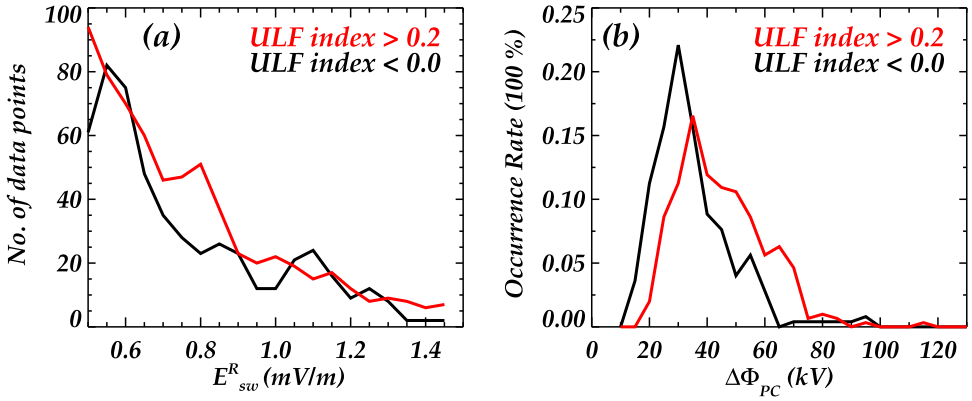

Figure 4. (a) Distribution of the number of data points in E^R_{sw}. (b) Relative occurrence rate of the same data points used in Figure 4a in $\Delta\Phi_{pc}$. Red denotes the data set associated with higher ULF index (>0.2), and black with lower ULF index (<0.0). Both data sets satisfy the conditions of $B_z > 1.5$ nT, P_{sw} = 2–3nPa with $\sigma < 0.5$, and E^R_{sw} = 0.5–1.5 mV/m.

suggesting a positive effect of IMF ULF power on the polar cap potential drop, independent of the solar wind speed effect.

[15] To determine whether solar wind dynamic pressure (P_{sw}), and not ULF activity, might lead to the effect seen in Figure 2, we collect those data points in Figure 2 that additionally satisfy a specific solar wind pressure condition, i.e., either P_{sw} = 2–3 nPa with $\sigma < 0.5$ or P_{sw} = 3–4 nPa with $\sigma <$ 0.7 where σ is the standard deviation. Twenty-two data points in each running average are used to calculate σ. This constraint is imposed to avoid windows that include a sudden change in pressure. From the data points satisfying this additional P_{sw} constraint, Figure 3 now illustrates the relationship between the ULF index and $\Delta\Phi_{pc}$ with the effects of V_{sw} and P_{sw} controlled. The left and the right panel of Figure 3 shows the result for lower (P_{sw} = 2–3 nPa with $\sigma <$ 0.5) and higher (P_{sw} = 3–4 nPa with $\sigma < 0.7$) dynamic pressure condition, with the symbol "Δ" and "+," respectively. The colors denote the different corresponding V_{sw}, and solid and dashed lines give linear fits for P_{sw} = 2–3 nPa with $\sigma < 0.5$ or P_{sw} = 3–4 nPa with $\sigma < 0.7$, respectively. Due to the rigorous data constrains the data points are sparse in Figure 3. Nevertheless, we can see the ULF effect, i. e., regardless of the colors (representing V_{sw}) and symbols (P_{sw}), there is a trend that larger $\Delta\Phi_{pc}$ is associated with larger ULF index. For example, one can tell a linear trend for both orange "Δ" and "+," and also for other colors, as indicated by solid and dashed lines. While the positive linear trend is seen for the majority of the fits in Figure 3, it is not seen for some of the selected cases (e.g., red "+," cyan "+," and black "Δ"). This can be attributed to the limited number of data points as well as uncertainties of AMIE potentials and the ULF wave index. Additionally, it is worth noting that the ULF index reflects not only ULF wave activity, but also other IMF irregularities such as discontinuities.

[16] We can also see the effects of V_{sw} and P_{sw} in Figure 3. The warm colors appear above the cold colors, showing a larger $\Delta\Phi_{pc}$ for larger V_{sw} regardless of the ULF index. Also, the "+" symbols tend to appear on the right and above the "Δ" symbols for the same color, indicating a larger $\Delta\Phi_{pc}$ for higher P_{sw} and larger ULF index.

[17] We calculate a partial correlation coefficient between the ULF index and $\Delta\Phi_{pc}$ after removing the effect of both V_{sw} and P_{sw} by successively doing a linear regression of ULF index and $\Delta\Phi_{pc}$ on the two solar wind parameters and subtracting the fit from the original values. From the data set satisfying condition A ($B_z > 1.5$ nT and $|B_y| < B_z$), the partial correlation coefficient is 0.19 with a p-value of 2×10^{-6}. The p-value, which is used to test statistical significance, is the probability (ranging from 0 to 1) of obtaining the same correlation coefficient by chance. Thus, the very low p-value indicates that it is highly unlikely that the positive correlation was obtained by chance. The relatively small partial correlation coefficient is due to the effects of V_{sw}, and P_{sw}, but also may be attributed to the highly structured convection patterns. We often observe highly structured convection flow patterns with a number of localized vortices under fluctuating northward IMF. For such a convection configuration, it is hard to estimate properly the electric potential drop across the polar cap. Also, due to the vortices, the enhanced flows that may be associated with IMF fluctuations do not necessarily yield a large potential drop. Thus, the effect of ULF fluctuations might be substantially greater than indicated by this partial correlation coefficient.

[18] Another way to examine the isolated effect from ULF fluctuations is to compare two data sets that are associated with different ULF power levels but satisfy the same solar wind conditions, i.e., P_{sw} = 2–3 nPa with $\sigma < 0.5$ and E^R_{sw} = 0.5–1.5 mV/m. Here, E^R_{sw} is the solar wind reconnection electric field [*Kan and Lee*, 1979], which has a strong correlation with $\Delta\Phi_{pc}$ and is given by

$$E^R_{sw} = -V_x \cdot \sqrt{B_y^2 + B_z^2}\,\sin^2(\theta/2),$$

where V_x is the x-component of the solar wind velocity, B_y and B_z are the y and z components of IMF, and $\theta = \arctan(B_y/B_z)$. Note that E^R_{sw} takes effects from both V_{sw} and IMF into account simultaneously. Again, we examine the case of northward IMF (with the constraint of $B_z >$ 1.5 nT). Figure 4a shows the distribution in E^R_{sw} of the data points that are associated with either lower ULF wave power (ULF index < 0.0 in black) or higher power (ULF index > 0.2 in red), respectively. In the range of 0.5–1.5 mV/m, the

distribution in E^R_{sw} is similar for the two data sets and has almost the same average P_{sw} (~2.44 nPa). However, distributions of the $\Delta\Phi_{pc}$ of the same data sets are quite different, with the one associated with a higher ULF power present at larger polar cap potentials, as shown in Figure 4b. This indicates that an overall increase of polar cap potentials occurs under enhanced fluctuating IMF conditions, independent of the increases that occur with increasing P_{sw} as well as with V_{sw}.

4. Summary and Conclusion

[19] We have conducted a statistical study to investigate the effect of IMF ULF power on the cross polar cap potential drop, primarily focusing on northward IMF. The analysis shows that the average $\Delta\Phi_{pc}$ increases roughly linearly with the ULF index, independent of the effects of V_{sw} and P_{sw}. The convection pattern is in general highly structured under fluctuating northward IMF, often accompanied by a number of localized vortices. Due to the vortices, the enhanced flows that may be associated with IMF fluctuations do not necessarily yield a large potential drop. Thus, despite the relatively small correlation coefficient (partial correlation coefficient of 0.19), the linear trend we have found supports the significant role of ULF fluctuations on the coupling of the solar wind to the magnetosphere-ionosphere system.

[20] We also examined the isolated effect of IMF ULF power by comparing two data sets that are associated with a lower and a higher ULF power level but satisfy the same conditions of P_{sw} and E^R_{sw}. We observed a substantially greater number of large polar cap potentials for the data set associated with a higher ULF power, which further supports there being a substantial effect of IMF ULF power on $\Delta\Phi_{pc}$.

[21] These statistical results support the previous finding by *Kim et al.* [2009] and *Lyons et al.* [2009] that, in addition to the well-established contributions from the IMF and the solar wind dynamic pressure, ULF fluctuations can be a potentially important additional driver of the strength of high latitude ionospheric convection and thus of coupling with the solar wind. Future studies will include understanding of how the solar wind fluctuations drive convection enhancements with highly structured flow patterns, which may need to include how the fluctuations are manifested within the magnetosheath and the effects of coupling with the ionosphere. It will be particularly interesting if we find that the fluctuations can often be associated with enough energy transfer to the magnetosphere to lead to the growth and expansion phase of substorms under conditions when such energy transfer would not otherwise be expected.

[22] **Acknowledgments.** This work was supported in part at UCLA by NASA grants NNX09AJ72G, NNX06AB89G, and NNX08AM46G, and work on the ULF index by V. Pilipenko at Augsburg College was supported by NSF grant ATM-0827903.

[23] Philippa Browning thanks the reviewers for their assistance in evaluating this paper.

References

Boudouridis, A., E. Zesta, L. R. Lyons, P. C. Anderson, and D. Lummerzheim (2005), Enhanced solar wind geoeffectiveness after a sudden increase in dynamic pressure during southward IMF orientation, *J. Geophys. Res.*, *110*, A05214, doi:10.1029/2004JA010704.

Boyle, C. B., P. H. Reiff, and M. R. Hairston (1997), Empirical polar cap potentials, *J. Geophys. Res.*, *102*(A1), 111–125, doi:10.1029/96JA01742.

Cowley, S. W. H. (1984), Solar wind control of magnetospheric convection, in *Achievements of the International Magnetospheric Study (IMS)*, edited by B. Battrick and E. Rolfe, pp. 483–494, Eur. Space Agency, Noordwijk, Netherlands.

Kan, J., and L. Lee (1979), Energy coupling function and solar wind magnetosphere dynamo, *Geophys. Res. Lett.*, *6*, 577–580, doi:10.1029/GL006i007p00577.

Kim, H.-J., L. R. Lyons, S. Zou, A. Boudouridis, D.-Y. Lee, C. Heinselman, and M. McCready (2009), Evidence that solar wind fluctuations substantially affect the strength of dayside ionospheric convection, *J. Geophys. Res.*, *114*, A11305, doi:10.1029/2009JA014280.

Kivelson, M. G., and A. J. Ridley (2008), Saturation of the polar cap potential: Inference from Alfven wing arguments, *J. Geophys. Res.*, *113*, A05214, doi:10.1029/2007JA012302.

Kozyreva, O., V. Pilipenko, M. J. Engebretson, K. Yumoto, J. Watermann, and N. Romanova (2007), In search of a new ULF wave index: Comparison of Pc5 power with dynamics of geostationary relativistic electrons, *Planet. Space Sci.*, *55*, 755–769, doi:10.1016/j.pss.2006.03.013.

Lyons, L. R., et al. (2009), Evidence that solar wind fluctuations substantially affect global convection and substorm occurrence, *J. Geophys. Res.*, *114*, A11306, doi:10.1029/2009JA014281.

Reiff, P. H., and J. G. Luhmann (1986), Solar wind control of the polar-cap voltage, in *Solar Wind-Magnetosphere Coupling*, edited by Y. Kamide and J. A. Slavin, pp. 453–476, Terra Sci., Tokyo.

Reiff, P., R. Spiro, and T. Hill (1981), Dependence of polar cap potential drop on interplanetary parameters, *J. Geophys. Res.*, *86*(A9), 7639–7648, doi:10.1029/JA086iA09p07639.

Richmond, A., and Y. Kamide (1988), Mapping electrodynamic features of the high-latitude ionosphere from localized observations: Technique, *J. Geophys. Res.*, *93*(A6), 5741–5759, doi:10.1029/JA093iA06p05741.

Ridley, A. J., and E. A. Kihn (2004), Polar cap index comparisons with AMIE cross polar cap potential, electric field, and polar cap area energy coupling function and solar wind magnetosphere dynamo, *Geophys. Res. Lett.*, *31*, L07801, doi:10.1029/2003GL019113.

Ridley, A. J., G. Lu, C. R. Clauer, and V. O. Papitashvili (1998), A statistical study of the ionospheric convection response to changing interplanetary magnetic field conditions using the assimilative mapping of ionospheric electrodynamics technique, *J. Geophys. Res.*, *103*(A3), 4023–4039, doi:10.1029/97JA03328.

Weimer, D. R. (2004), Correction to "Predicting interplanetary magnetic field (IMF) propagation delay times using the minimum variance technique," *J. Geophys. Res.*, *109*, A12104, doi:10.1029/2004JA010691.

Weimer, D. R., D. M. Ober, N. C. Maynard, M. R. Collier, D. J. McComas, N. F. Ness, C. W. Smith, and J. Watermann (2003), Predicting interplanetary magnetic field (IMF) propagation delay times using the minimum variance technique, *J. Geophys. Res.*, *108*(A1), 1026, doi:10.1029/2002JA009405.

A. Boudouridis, Space Science Institute, 4750 Walnut St., Ste. 205, Boulder, CO 80301, USA.

H.-J. Kim and L. Lyons, Department of Atmospheric and Oceanic Sciences, University of California, Los Angeles, CA 90095-1565, USA. (heekim@atmos.ucla.edu)

V. Pilipenko, Space Research Institute, Moscow 117810, Russia.

A. J. Ridley, Center for Space Environment Modeling, University of Michigan, Ann Arbor, MI 48109, USA.

J. M. Weygand, IGPP, University of California, 3845 Slichter Hall, Los Angeles, CA 90095-1567, USA.